Energy & Environmental Science

Cite this: *Energy Environ. Sci.*, 2012, **5**, 6872

www.rsc.org/ees

COMMUNICATION

Atomic layer deposition of vanadium oxide on carbon nanotubes for high-power supercapacitor electrodes

Sofiane Boukhalfa, Kara Evanoff and Gleb Yushin*

Received 12th January 2012, Accepted 21st February 2012
DOI: 10.1039/c2ee21110f

Vanadium oxides may offer high pseudocapacitance but limited electrical conductivity and specific surface area. Atomic layer deposition allowed uniform deposition of smooth nanostructured vanadium oxide coatings on the surface of multi-walled carbon nanotube (MWCNT) electrodes, thus offering a novel route for the formation of binder-free flexible composite electrode fabric for supercapacitor applications with large thickness, controlled porosity, greatly improved electrical conductivity and cycle stability. Electrochemical measurements revealed stable performance of the selected MWCNT–vanadium oxide electrodes and remarkable capacitance of up to ~1550 F g^{-1} per active mass of the vanadium oxide and up to ~600 F g^{-1} per mass of the composite electrode, significantly exceeding specific capacitance of commercially used activated carbons (100–150 F g^{-1}). Electrochemical performance of the oxide layers was found to strongly depend on the coating thickness.

Introduction

Supercapacitors, also called electrochemical capacitors (EC), are rechargeable electrochemical energy storage devices, which offer a much longer life cycle and higher power density than batteries.[1] As such, supercapacitors can replace or complement batteries in various applications, ranging from hybrid electrical engines for vehicles to pulse-power applications in the aerospace and defense industries.

Two types of supercapacitors exist: electrical double-layer capacitors with carbon electrodes and pseudocapacitors with metal-oxide or conducting polymer electrodes. Transition metal-oxides exhibit fast and electrochemically reversible Faradaic redox reactions to store charge in supercapacitors, resulting in high capacitance, but often suffer from low surface area and low electrical conductivity. The only metal-oxide with both high capacitance (3–4 times higher than porous carbons) and conductivity is ruthenium oxide (the "original" supercapacitor),[2,3] but its high cost is prohibitive to most commercial applications. As such, research into inexpensive materials for use in supercapacitors is critical to ensure that the future demand for high power density energy storage devices can be met.

Among various transition metal oxides, vanadium oxides have received relatively modest attention for supercapacitor applications.[4–15] Yet, this material is abundant, relatively inexpensive (~$12 per kg), and offers a broad range of oxidation states which will offer the broad range of redox reactions suitable for supercapacitor operation. Specific capacitance of vanadium oxide is known to depend on the preparation conditions and its morphology. It also strongly depends on the measurement technique (measurements in a symmetric two-electrode cell configuration *vs.* individual electrode measurements in a three-electrode cell configuration). The difference by the factor of 3 or more between such measurements is common if the redox peaks in the positive and negative electrodes of the two-electrode cell do not take place at the same value of the applied voltage. When referenced to the ultimate device performance, the

Department of Materials Science and Engineering, Georgia Institute of Technology, Atlanta, GA, USA. E-mail: gleb.yushin@mse.gatech.edu

Broader context

With the advent of modern electronics, electrical vehicles and smart grids, energy storage and conversion are becoming increasingly important. High power and high energy storage devices such as supercapacitors are needed for providing pulse power in applications ranging from wind turbines to hybrid engines, which will decrease our current dependence on environmentally harmful fossil fuels. There is a critical need to develop novel supercapacitor electrodes with improved high-energy and high-power characteristics. The formation of carbon–transition metal oxide nanocomposites may offer unique benefits for such applications. Broadly available transition metal oxides, such as vanadium oxide, offer high ion storage capabilities due to the broad range of their oxidation states, but suffer from high resistivities. MWCNTs, in contrast, are not capable to store high ion content, but offer high and readily accessible surface area and high electrical conductivity. By exploiting the ability of atomic layer deposition to produce uniform coatings of metal oxides on MWCNT electrodes, we demonstrate an effective way to produce high-power supercapacitor electrodes with ultra-high energy capability.

three-electrode measurements will give an over-estimated capacitance value unless the second electrode prepared from a different material can offer identical or higher capacitance. The two-electrode measurements, in contrast, will give an under-estimated performance because the symmetric electrodes are commonly not balanced and not optimized, particularly those that are based on Faradaic reactions.[16]

Several types of vanadium oxide-based electrodes have been previously investigated. Pure V_2O_5 with enhanced surface area prepared by co-precipitation and calcinations[11] or *via* formation of sol–gel[12] or *via* electrodeposition[15] offers moderately high capacitance (200–260 F g^{-1}) and high resistance in aqueous (KCl) electrolyte when evaluated in a three-electrode configuration. The highest capacitance was reported for vanadium oxide aerogels (960–2000 F g^{-1}).[6–9] It is important to note, however, that these results were obtained at extremely slow scan rates (0.1 mV s^{-1}) on very small samples using a "sticky carbon" method, applicable in a research setting only.

To compensate for the very low electrical conductivity of vanadium oxide (VO_x), the use of surface-oxidized vanadium nitride nanoparticles was proposed.[17] The produced electrodes, however, demonstrated poor power performance, presumably due to high particle-to-particle resistance. Carbon may offer higher electrical conductivity and higher specific surface area than vanadium nitride. Synthesis of carbon–vanadium oxide composites *via* a solid-state reaction process between VO_2 and ordered mesoporous carbons did not allow sufficient control over the composite microstructure at the nano-scale and thus a relatively moderate capacitance value (131 F g^{-1}) was achieved.[13]

In a recent study, vacuum filtration was used to combine V_2O_5 nanowires and carbon nanotubes (CNTs) to form binder-free supercapacitor electrodes. While the obtained results were promising, only moderate values of capacitance and relatively low power characteristics of the electrodes were achieved.[18] By using other approaches which provide uniform coating of metal oxides on carbon materials, electrodes with higher energy and power densities could be fabricated.

Electrodeposition of thin layers of vanadium oxide on the surface of either platinum (Pt) or ultra-thin carbon nanotube (CNT) electrodes resulted in an impressive specific capacitance of 170–900 F g^{-1} when measured in a three electrode configuration using a Li-ion battery-type electrolyte ($LiClO_4$ salt dissolved in propylene carbonate, PC).[4] While the obtained results are very promising, some possible limitations of the electrodeposition include the corrosive nature of the deposition electrolyte and limited uniformity of the deposited oxide layer. The lack of uniformity resulted in low capacitance retention at fast scan rates and current densities.[4]

Vapor deposition routes may offer an alternative solution for the oxide deposition. Atomic layer deposition (ALD),[19–21] in particular, offers a combination of unique advantages. In ALD, the precursor and other source vapors are pulsed into the chamber one at a time, separated by purging or evacuation periods. Each pulse step commonly deposits a sub-monomolecular layer of the precursor onto the substrate, while the purge or evacuation step limits the reaction to the surface by removing the excess reaction gases. As such, ALD allows precise, uniform and conformal deposition of oxide coatings on porous substrate surfaces, provided enough time is allocated for the diffusion of the precursor gases into (out of) the porous structure of the substrate during both the pulse and purge periods. Another advantage of ALD is a low synthesis temperature which facilitates deposition of coatings on fabric or fiber substrates for wearable or multifunctional energy storage devices.[22–24] While ALD tools are currently expensive, several companies including Levitech (Netherlands) are developing low-cost large-size ALD reactors for a growing number of emerging applications. While the use of ALD has been explored for thin film batteries[21] and gas sensing applications,[20] it has not been utilized for the fabrication of high energy density supercapacitor electrodes.

Several studies reported the use of thin free-standing CNT films as low capacitance but high-rate electrodes for high-power supercapacitor applications.[25–29] In this work for the first time we conformally deposited vanadium oxide coatings of various thicknesses on the internal surface area of porous CNT electrodes using the ALD technique and evaluated the composite performance for use in supercapacitors. We have systematically studied the structural, electrical, and electrochemical properties of the produced nanocomposite electrodes as a function of the coating thickness. The proposed technique can be utilized for the fabrication of both on-chip and wearable supercapacitors and electrochemical sensors. In such composites, CNTs provide high electrical and thermal conductivity while ALD-deposited oxide coating increases the electrode capacitance by more than an order of magnitude.

Experimental

Multi-walled CNTs were grown *via* a 5 min $FeCl_2$ catalyst-assisted chemical vapor deposition (CVD) process at 820 °C using an acetylene precursor.[30] In order to prepare uniform stand-alone CNT electrodes, vertically aligned CNTs were separated from the substrate and boiled at 100 °C in a 1 : 1 mixture of concentrated sulfuric and nitric acid (1 mg of CNT per 1 mL of the solution) under a condenser for 1 h. This acid treatment opens the CNT caps and induces defects and multiple carboxylic groups on the CNT surface, which serve as nucleation sites for the subsequent oxide deposition and increase the rate of electron transfer. The CNT-containing solution was then diluted with de-ionized H_2O (DI, 18 MΩ) and vacuum filtered through a grade 2 Whatman filter (Whatman, USA). Ethanol was used to remove the acid residues and stop the oxidation process. The CNT electrodes were then dried overnight in a vacuum oven at 80 °C. The acid purification step also allows for the formation of a binder-free, flexible, and free-standing CNT electrode, since the filtered nanotubes form a three dimensional (3D) porous network of entangled and well-bonded CNTs. Similar processes could be used to deposit well-adhered CNTs on the surface of various fabrics.[22] These electrodes were used as substrates for deposition of vanadium oxide *via* ALD.

ALD deposition was done in a custom-built ALD system consisting of a quartz tube (heated in a furnace) through which precursor vapors were introduced alternately. Vanadium tri-*n*-propoxide oxide (Gelest, Inc., USA) and DI H_2O (18 MΩ) were used as precursors and were heated to ~45 °C and 100 °C, respectively, during the deposition. High purity Ar (99.999%, Air Gas, USA) was used as both carrier and purging gas (residence and purging periods were 10 s and 20 s, respectively for the H_2O precursor and for the vanadium precursor). All the precursor gas lines were maintained at 100 °C during the deposition process. The pressure of the system was maintained at 4 Torr throughout the deposition. The temperature of the furnace was maintained at 170–190 °C.

X-Ray diffraction (XRD) experiments using Cu-K_α radiation were performed with an X'Pert PRO Alpha-1 diffractometer (Panalytical, USA) equipped with a monochromator. Scanning electron microscopy (SEM) measurements of the nanowire morphology and tube diameter were performed using a LEO 1550 microscope (Carl Zeiss, Germany). ImageJ software was employed for the SEM image analysis to determine the nanowire diameter distributions. Raman experiments were performed on an Alpha 300 spectrometer (WITec, Germany) excited using a 514 nm wavelength laser with a 50× objective. The intensity of the laser was 215 μW at the sample surface and the laser spot size was <5 μm. Spectra were acquired by accumulating 30 of 1s spectra.

The mass ratios of CNT and the oxide in the VO_x–CNT composites were estimated using thermogravimetric analysis (TGA) performed in an oxidizing atmosphere of air by detecting the burning off of the CNT at around 400–600 °C. Such measurements were performed using a Q50 Thermogravimetric analyzer (TA Instruments, USA). TGA measurements were performed on the samples by heating them from room temperature to 900 °C at a 5 °C min^{-1} ramping rate in a Pt pan. Air was flown over the samples at 10 mL min^{-1}.

Four types of samples were investigated through the course of this study. An uncoated CNT electrode sample was compared with CNT samples coated with vanadium oxide deposited through 100, 300, and 500 ALD cycles. For electrochemical testing, the coated electrodes were split into two near-identical electrodes of ~80 μm in average thickness, with each electrode attached to a current collector foil by the "split" side. All electrodes were of ~0.25 cm^2 geometrical area. All electrochemical tests have been performed in fully symmetric two-electrode configuration using beaker-type cells, Au current collectors (Sigma-Aldrich, USA) and a 25 μm thick GorTex separator (GorTex, USA). We selected 8 M LiCl solution (Sigma-Aldrich, USA) as an electrolyte because of vanadium oxide's high solubility in other aqueous electrolytes, such as 0.5 M H_2SO_4 electrolyte. In contrast, previous experiments[11] showed good stability and negligible solubility of V_2O_5 supercapacitor electrodes in LiCl.

Electrochemical characterization was performed using galvanostatic (constant current) charge–discharge (C–D) measurements, electrochemical impedance spectroscopy (EIS), and cyclic voltammetry (CV). Cyclic voltammetry was performed using a Solartron 1480A (AMETEK Advanced Measurement Technology, USA) with the potential being swept from −0.6 V to +0.6 V at scan rates of 5–1000 mV s^{-1}. The integrated-average gravimetric capacitance of each electrode was calculated from the CV data according to:

$$C_{\text{electrode}} = 2C_{\text{cell}} = \left(\frac{2}{(\mathrm{d}U/\mathrm{d}t)m}\right)\left\{\int_{-0.6\text{V}}^{0.6\text{V}} I(U)\mathrm{d}U - \int_{0.6\text{V}}^{-0.6\text{V}} I(U)\mathrm{d}U\right\}\frac{1}{2}\frac{1}{1.2\text{V}},$$

where dU/dt is the scan rate, m is the mass of each electrode in a symmetric cell, and $I(U)$ is the total current. The *C–D* tests were carried out using an Arbin SCTS supercapacitor testing system (Arbin Instruments, TX, USA) between −0.6 V and +0.6 V at charge/discharge current densities between 1000 and 20 000 m Ag^{-1}, based on the mass of a single electrode. The gravimetric capacitance was deduced from the average slope of the discharge curve according to:

$$C_{\text{electrode}} = 2C_{\text{cell}} = \left(\frac{2I}{(\mathrm{d}U/\mathrm{d}t)m}\right),$$

where I is the total current, dU/dt is the slope of the discharge curve, and m is the mass of each electrode in a symmetric cell. EIS measurements were performed on a Gamry Potentiostat from 100 kHz to 1 mHz at 1 V scanning amplitude. All supercapacitors were tested in the following order to ensure reproducibility and accuracy: CV (at scan rates increasing from 5 to 1000 mV s^{-1}) was followed by *C–D* (at current densities increasing from 1 to 20 A g^{-1}) and EIS (at frequencies decreasing from 100 kHz to 1 mHz).

Results and discussion

SEM studies (Fig. 1) showed a very high degree of coating uniformity throughout the electrodes. Even for the largest number of ALD cycles (500 cycles) the CNTs appear to be conformally coated with an oxide layer and no clusters are seen blocking the electrode pores. Since in an ideal case ALD is a surface-limited process, the average coating thickness or the average tube diameter should increase proportionally to the number of the ALD cycles. Software analysis of multiple SEM micrographs confirmed this and showed a linear increase in the average CNT diameter from ~70 nm (for bare CNTs) to ~180 nm (after 500 ALD cycles) (Fig. 2), suggesting that the time allocated for the diffusion of the precursor gases into the porous structure in each cycle was sufficient for the reaction to be surface kinetics-controlled. The average coating thickness increases by 0.1 nm per cycle.

A shoulder in the (002) carbon peak present in the XRD of CNT samples (Fig. 3a) may be related to the variation in the spacing between the tube walls. XRD measurements of the as-deposited oxide films showed both amorphous and nano-crystalline features, but did not allow us to unambiguously identify the present phases due to the small peak intensity, large peak width and similarity in the spectral position of the reflections corresponding to different phases (Fig. 3a). Vanadium oxide possesses numerous oxidation states, with the most common phases being VO, V_2O_3, VO_2, V_2O_5 and V_6O_{13}. Comparison of the recorded patterns with literature[31–35] suggests the presence of all these phases. The color of the coated electrode is in between green (typical for VO_2) and yellow (typical for V_2O_5).

Raman spectroscopy was also used to characterize the purity and the degree of disorder in the starting CNT electrode and further verify the presence of different phases in the ALD-deposited VO_x coatings (Fig. 3b). Perfect graphite clearly shows only one Raman active mode, the G-band, located at 1582 cm^{-1} and corresponding in-plane vibrations.[36] Defective graphite, CNTs and disordered carbons show an additional band at ~1360 cm^{-1} (D-band) associated with a double-resonance Raman process.[37] The low value of the ratio of the integrated intensities of D and G bands (I_D/I_G) (in our case ~0.9) and high intensity of the G′′ band at ~2710 cm^{-1} indicate high CNT purity and low concentration of defects in the inner tubes of the oxidized multi-walled CNTs.[36]

The VO_x-coated samples exhibit several additional peaks in the 200–1000 cm^{-1} region, as expected from previous studies.[35,38] The first two peaks occurring at 267 cm^{-1} and at 406 cm^{-1} are attributed to bending vibrations due to the V=O bond. This is supported by the presence of the small peak at 1017 cm^{-1}, which is also indicative of a V=O bond. The peak occurring at 511 cm^{-1} is attributed to a V_3–O (triply coordinated oxygen) bond. Finally, the peak at 712 cm^{-1} is

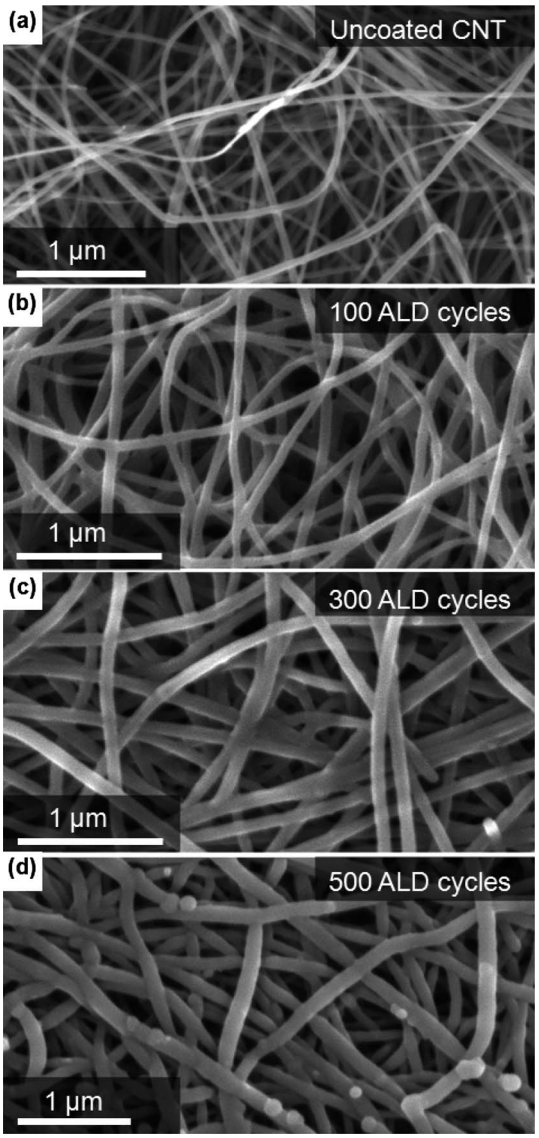

Fig. 1 SEM images of (a) uncoated samples, and samples coated with VO_x for (b) 100 ALD cycles, (c) 300 ALD cycles, and (d) 500 ALD cycles.

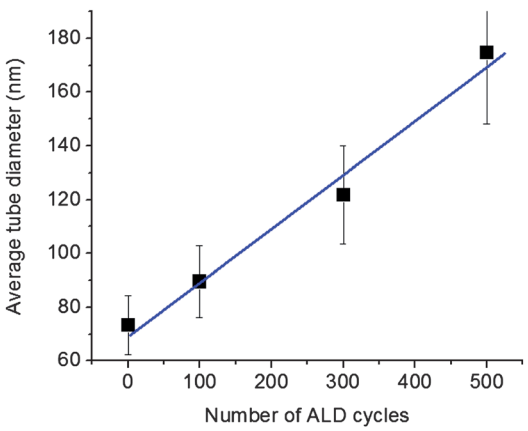

Fig. 2 Changes in the average tube diameters with cycle number. The data were extracted by the analysis of SEM micrographs.

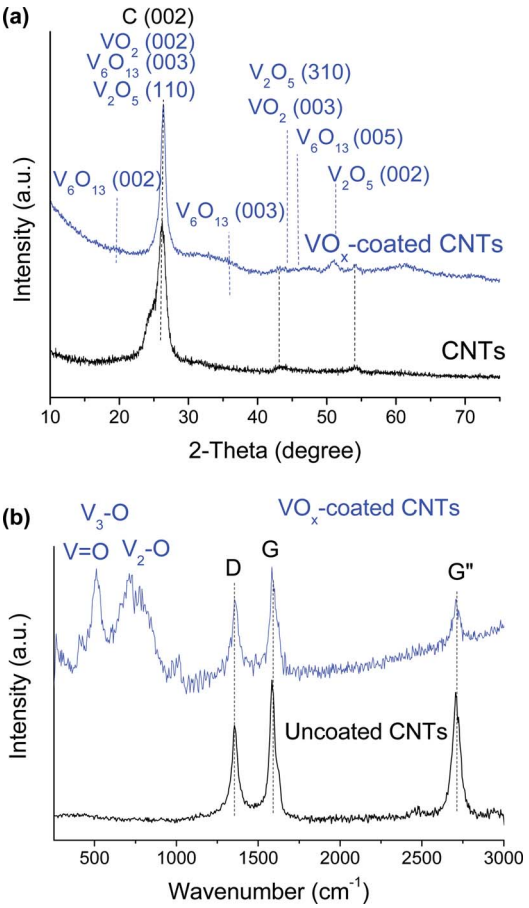

Fig. 3 Studies of VO_x-coated and uncoated CNT samples: (a) XRD and (b) Raman spectroscopy.

attributed to a V_2–O (doubly coordinated oxygen) bond. It is important to note that V═O bonds are present in VO_2, V_2O_5, and V_2O_3. Triply coordinated V_3–O bonds only appear in the chemical structure of V_2O_5, while doubly coordinated V_2–O bonds are present in the chemical structure of VO_2 and V_2O_3. These findings further suggest the presence of nanocrystalline regions of different vanadium oxide phases.

CV graphs of CNT electrodes before and after coating with VO_x of different thicknesses (Fig. 4) reveal a significant impact of the sample preparation conditions on both the shape of the curves and their relative changes with increasing sweep rate. The bare CNT electrode exhibits specific capacitance of ~30 F g^{-1} (Fig. 4a), consistent with previous measurements.[25–29,39] In spite of the surface oxidation, CNTs do not show evident redox peaks. Furthermore, the capacitance of CNT electrodes shows little changes in the range of sweep rates from 5 to 500 mV s^{-1}, which indicates high-power performance capability and is likely due to the high electrical conductivity of CNTs and large interconnected mesopores present in this sample.

After exposure to 100 ALD cycles and being coated with ~10 nm of VO_x, the symmetric supercapacitor increases its capacitance and energy density by more than an order of magnitude (Fig. 4b). Interestingly, we can distinguish two types of pseudo-capacitive behavior in VO_x-coated samples: (i) a broad peak in the central region which is typical for battery-like Faradaic reactions of intercalating compounds and (ii) a nearly rectangular background

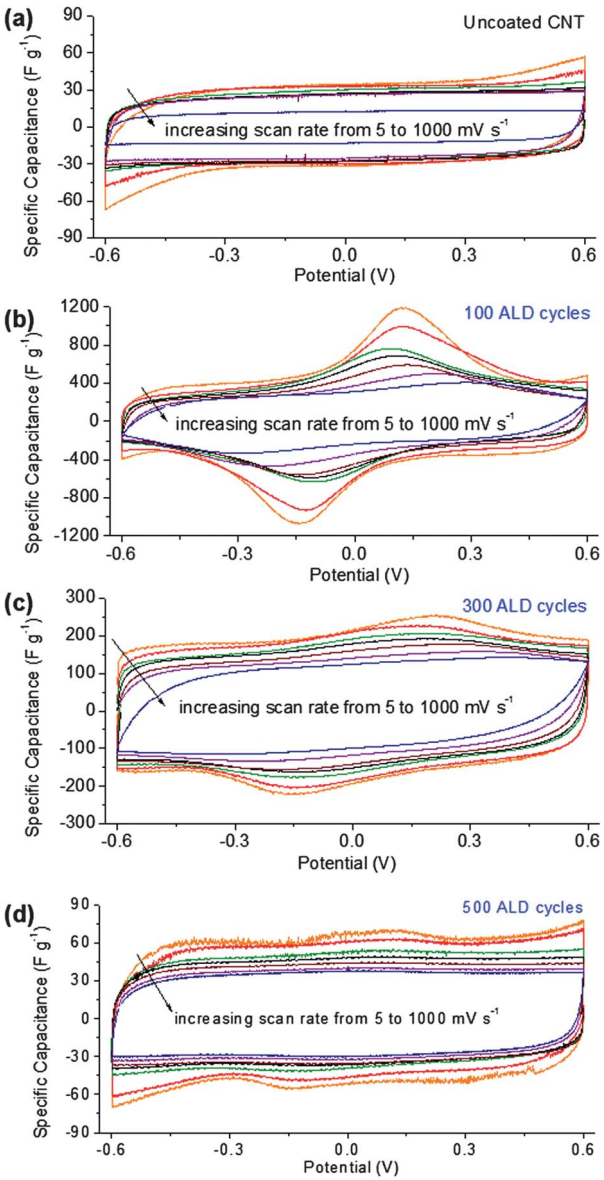

Fig. 4 Cyclic voltammograms of CNT electrodes: (a) uncoated, (b) exposed to 100 ALD cycles, (c), 300 cycles and (d) 500 cycles at different scan rates in the range of 5–1000 mV s^{-1}.

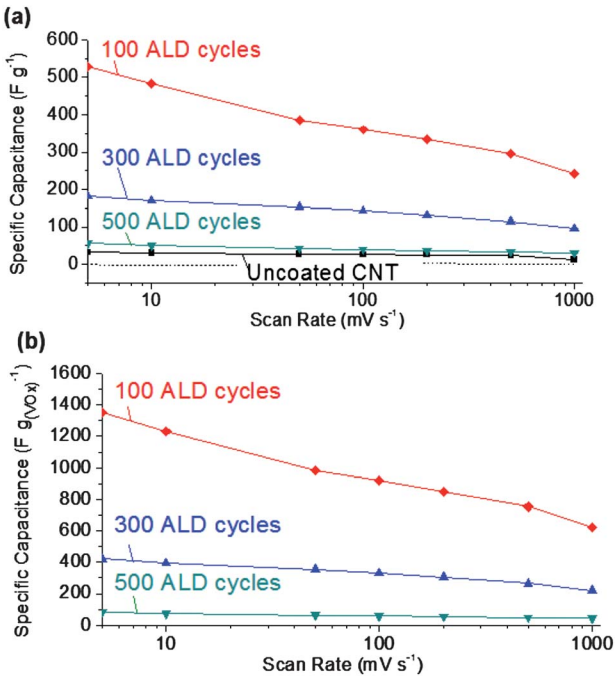

Fig. 5 Changes in the specific capacitance of the produced samples for: (a) composite electrode and (b) contribution of VO_x coating.

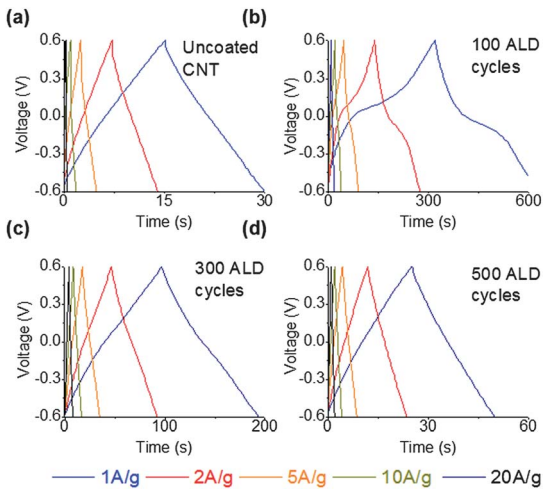

Fig. 6 Charge–discharge profiles of the produced samples: (a) uncoated CNT electrodes, (b) exposed to 100 ALD cycles, (c) 300 cycles and (d) 500 cycles for current density in the range of 1–20 A g^{-1}.

(~300 F g^{-1}) which is typical for an ideal pseudocapacitor-like materials, including hydrous ruthenium oxide.[3] As expected, the height of the battery-like redox peak diminishes rapidly with increasing sweep rate, while the rectangular background exhibits little change, indicating a very high rate of the pseudocapacitive reactions between the deposited VO_x coating and the electrolyte. This, in turn, suggests very good promise of the hydrous vanadium oxide for high energy/high-power supercapacitor applications.

Increasing the VO_x coating thickness by exposing the surface-oxidized CNTs to 300 (Fig. 4c) and 500 (Fig. 4d) ALD cycles decreases the capacitance value significantly. The rectangular background decreases by two and six times, respectively, while the central battery-like peak disappears almost completely. This behavior can be explained by the contributions of three separate phenomena: (i) by the presence of active redox sites only in the top surface layer of VO_x coatings, (ii) by a limited access of the electrolyte ions to the bulk of the coating, and (iii) by a decrease in the electron transport to the active redox sites due to the increase in thickness of electrically insulative coating. Indeed, all redox reactions require the presence of both ions and electrical carriers (electrons or holes) near the active site and the increase in the coating thickness likely impedes the transport of both: electrons from the CNT and ions from the electrolyte. We further propose that the top layer of the coating unlikely exhibits higher concentration of active sites because ALD processes are known to produce rather uniform structure. At the same time, the interface between the CNT and the coating (being a non-coherent interface) may increase the specific volume, concentration of vacancies, nano-sized voids and defects in this region of the coating, and

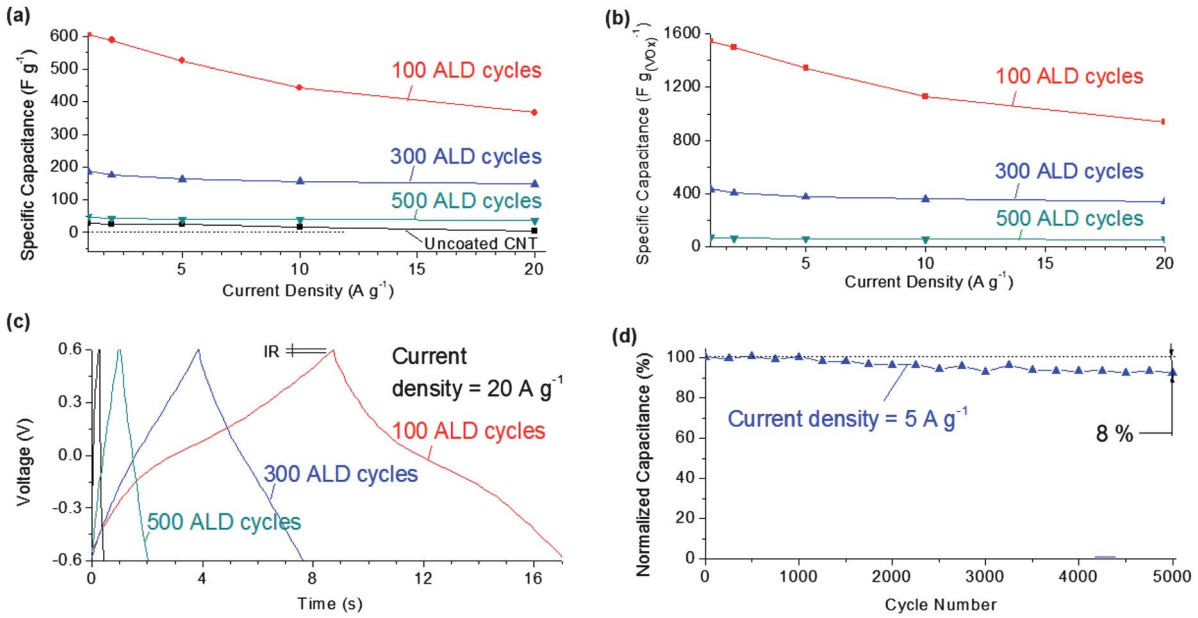

Fig. 7 Changes in the specific capacitance of the produced electrode samples for: (a) composite electrode and (b) contribution of VO_x coating as a function of current density. (c) Charge–discharge profiles of the produced electrodes at the current density of 20 A g^{-1}. (d) A typical capacitance retention of VO_x coating as a function of charge–discharge cycle numbers.

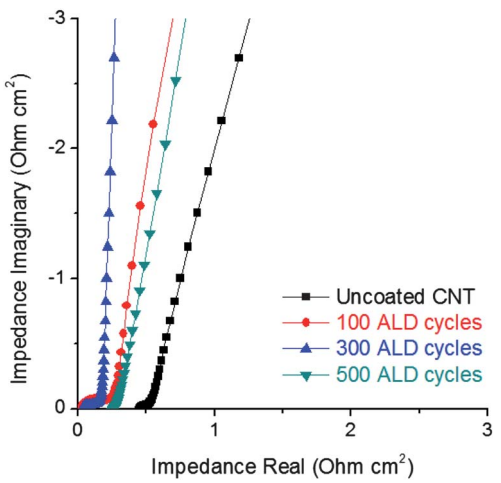

Fig. 8 Nyquist plots of the produced electrode samples.

thus may potentially offer higher concentration of active redox sites than both the bulk and the top coating layer. However, while we cannot exclude the possibility that the defects at the carbon–oxide interface favor higher pseudocapacitance, we could not detect significant structural differences between the coatings using the Raman spectroscopy studies.

Fig. 5 summarizes results of the CV measurements. While all the coated CNT electrodes offer higher capacitance than bare CNT, the electrodes with the thinnest coating of ~10 nm offer the best performance with the specific capacitance of the composite approaching ~530 F g^{-1} at 5 mV s^{-1}. Even at the ultra-high sweep rate of 1000 mV s^{-1} the capacitance remains higher than 240 mV s^{-1}, which is unmatched even by the most advanced porous carbon electrodes of comparable thickness.[40–47] Furthermore, the capacitance of the VO_x coating alone approaches 1400 F g^{-1} at 5 mV s^{-1}. This is one of the highest capacitance values for any metal oxide measured in aqueous electrolytes in a symmetric two-electrode configuration. It exceeds the performance of hydrous manganese oxide and ruthenium oxide.[2,3,48]

C–D measurements (Fig. 6) reveal similar trends. Except for the sample produced with 100 ALD cycles, the electrodes show relatively linear profiles, characteristic of ideal capacitor behavior. Fig. 7a and b show capacitance retention of the electrodes at increasing current density. Due to the slow reactions at the battery-like redox sites (Fig. 4b), the sample produced with 100 ALD cycles shows the lowest power characteristics. Nonetheless, the capacitance of this sample remains above 360 F g^{-1} even at a very high current density of 20 A g^{-1}. The slightly higher capacitance value for this sample obtained from C–D than from CV measurements is an artifact of the capacitance deduction procedures (see Experimental section) designed for samples exhibiting a near-ideal capacitive behavior. The C–D measurements also confirm the extremely low resistance of our electrodes. Even at a very high current density (20 A g^{-1}), the IR drop found at the onset of the discharge curve (Fig. 7c) is extremely small, which indicates the low value of the equivalent series resistance (ESR) for the symmetric supercapacitor and confirms the usability of the device for high power operations. Charge–discharge tests also showed a stable (for laboratory quality cells) performance (Fig. 7d).

The Nyquist plots (Fig. 8) extracted from the EIS measurements are typical for supercapacitors. A classical Nyquist plot contains two segments: the 45 degree segment at high frequency and the nearly vertical line at low frequency. The length of the 45 degree segment is related to the resistance faced by the ions during their transport into the core of the porous electrode. The very small length of this segment (~0.1 Ω cm^2) indicates rapid ion transport within all of our electrodes. An ESR is another important characteristic of a supercapacitor. It is measured at high frequency where the imaginary component of the complex impedance becomes zero. The contributions to ESR primarily include the electrical resistance of the electrodes and the

electrode–current collector interfaces. As expected from the C–D measurements, the ESR for all the samples is very low, ranging from as little as 0.025–0.4 Ω cm^2. In comparison, typical porous carbon powder-based supercapacitors exhibit ESR of 0.2–1 Ω cm^2.[39,41–43,46,47,49–51]

The low values of ESR in our devices are related to the interconnected network of highly conductive CNTs within our binder-free electrodes. Indeed, vanadium oxide coating was deposited after the CNT film preparation and thus it does not interfere with the very good electron transport at the occasional contact points between the individual CNTs. The lower ESR of the coated CNT electrodes was unexpected as the metal-oxide has significantly lower conductivity than the CNTs. We therefore postulate that the observed improvements are largely related to the lower impedance of the electrode–current collector interface between the gold foil and a more rigid vanadium oxide-reinforced CNT electrode containing individual CNTs perpendicular to the electrode surface (see Experimental details) and providing better electron transport. We also cannot exclude the possibility that vanadium oxide coating may increase the number of charge carriers at the metal oxide/CNT interface. The very small semi-circles observed at high frequencies are related to the parasitic capacitance at the electrode–current collector interface.[52–54]

Conclusions

ALD allows one to uniformly deposit metal oxides on porous CNT or carbon nanofiber electrodes, thus offering a novel route for the formation of binder-free supercapacitor electrodes with controlled porosity, greatly increased electrical conductivity, and specific capacitance. The ability to precisely control the coating thickness and microstructure permits systematic studies of the ion intercalation and diffusion into the bulk of the electrodes. Electrochemical measurements revealed stable performance of the vanadium oxide-coated CNT electrodes with excellent capacitance retention at high current densities or sweep rates. Decreasing the coating thickness to ~10 nm allows one to achieve very high capacitance of the vanadium oxide with values approaching ~1550 F g^{-1} at the current density of 1 A g^{-1}. Such high capacitance values are unprecedented for supercapacitor electrodes measured in a symmetrical two-electrode configuration in aqueous electrolytes. Our results indicate the importance of electrode uniformity, precise control over the conformity and thickness of the oxide coatings, and promise of the application of ALD techniques for supercapacitors. Our future efforts will focus on the application of ALD techniques to the deposition of other metal oxides, optimization of oxide layer microstructure, and the use of smaller diameter CNTs which are expected to further improve the specific capacitance of the composite electrodes.

Acknowledgements

This work was partially supported by AFOSR (grant # FA9550-09-1-0176) and ACS petroleum research fund (grant # 49045-DNI10).

References

1 P. Simon and Y. Gogotsi, Materials for electrochemical capacitors, *Nat. Mater.*, 2008, **7**(11), 845–854.
2 J. P. Zheng and T. R. Jow, A new charge storage mechanism for electrochemical capacitors, *J. Electrochem. Soc.*, 1995, **142**(1), L6–L8.
3 J. P. Zheng, P. J. Cygan and T. R. Jow, Hydrous ruthenium oxide as an electrode material for electrochemical capacitors, *J. Electrochem. Soc.*, 1995, **142**(8), 2699–2703.
4 I. H. Kim, J. H. Kim, B. W. Cho, Y. H. Lee and K. B. Kim, Synthesis and electrochemical characterization of vanadium oxide on carbon nanotube film substrate for pseudocapacitor applications, *J. Electrochem. Soc.*, 2006, **153**(6), A989–A996.
5 D. Sun, C. W. Kwon, G. Baure, E. Richman, J. MacLean, B. Dunn and S. H. Tolbert, The relationship between nanoscale structure and electrochemical properties of vanadium oxide nanorolls, *Adv. Funct. Mater.*, 2004, **14**(12), 1197–1204.
6 G. Sudant, E. Baudrin, B. Dunn and J. M. Tarascon, Synthesis and electrochemical properties of vanadium oxide aerogels prepared by a freeze-drying process, *J. Electrochem. Soc.*, 2004, **151**(5), A666–A671.
7 W. Dong, J. Sakamoto and B. Dunn, Electrochemical properties of vanadium oxide aerogels and aerogel nanocomposites, *J. Sol-Gel Sci. Technol.*, 2003, **26**(1–3), 641–644.
8 W. Dong, D. R. Rolison and B. Dunn, Electrochemical properties of high surface area vanadium oxide aerogels, *Electrochem. Solid-State Lett.*, 2000, **3**(10), 457–459.
9 D. R. Rolison and B. Dunn, Electrically conductive oxide aerogels: new materials in electrochemistry, *J. Mater. Chem.*, 2001, **11**(4), 963–980.
10 B. Wang, K. Konstantinov, D. Wexler, H. Liu and G. Wang, Synthesis of nanosized vanadium pentoxide/carbon composites by spray pyrolysis for electrochemical capacitor application, *Electrochim. Acta*, 2009, **54**(5), 1420–1425.
11 Z. J. Lao, K. Konstantinov, Y. Tournaire, S. H. Ng, G. X. Wang and H. K. Liu, Synthesis of vanadium pentoxide powders with enhanced surface-area for electrochemical capacitors, *J. Power Sources*, 2006, **162**(2), 1451–1454.
12 R. N. Reddy and R. G. Reddy, Porous structured vanadium oxide electrode material for electrochemical capacitors, *J. Power Sources*, 2006, **156**(2), 700–704.
13 L. Hu, L. Yu, C. Zhao, X. Long and W. Chen, Synthesis and characterization of VO(2)/mesoporous carbon composites for hybrid capacitors, *J. Wuhan Univ. Technol., Mater. Sci. Ed.*, 2010, **25**(4), 574–578.
14 Z. Chen, V. Augustyn, J. Wen, Y. W. Zhang, M. Q. Shen, B. Dunn and Y. F. Lu, High-performance supercapacitors based on intertwined CNT/V_2O_5 nanowire nanocomposites, *Adv. Mater.*, 2011, **23**(6), 791.
15 C.-M. Huang, C.-C. Hu, K.-H. Chang, J.-M. Li and Y.-F. Li, Pseudocapacitive characteristics of vanadium oxide deposits with a three-dimensional porous structure, *J. Electrochem. Soc.*, 2009, **156**(8), A667–A671.
16 V. Khomenko, E. Frackowiak and F. Beguin, Determination of the specific capacitance of conducting polymer/nanotubes composite electrodes using different cell configurations, *Electrochim. Acta*, 2005, **50**(12), 2499–2506.
17 D. Choi, G. E. Blomgren and P. N. Kumta, Fast and reversible surface redox reaction in nanocrystalline vanadium nitride supercapacitors, *Adv. Mater.*, 2006, **18**(9), 1178.
18 S. D. Perera, B. Patel, N. Nijem, K. Roodenko, O. Seitz, J. P. Ferraris, Y. J. Chabal and K. J. Balkus, Vanadium oxide nanowire–carbon nanotube binder-free flexible electrodes for supercapacitors., *Adv. Energy Mater.*, 2011, **1**(5), 936–945.
19 Y. S. Jung, A. S. Cavanagh, L. A. Riley, S. H. Kang, A. C. Dillon, M. D. Groner, S. M. George and S. H. Lee, Ultrathin direct atomic layer deposition on composite electrodes for highly durable and safe Li-ion batteries, *Adv. Mater.*, 2010, **22**(19), 2172.
20 M.-G. Willinger, G. Neri, E. Rauwel, A. Bonavita, G. Micali and N. Pinna, Vanadium oxide sensing layer grown on carbon nanotubes by a new atomic layer deposition process, *Nano Lett.*, 2008, **8**(12), 4201–4204.
21 K. Le Van, H. Groult, A. Mantoux, L. Perrigaud, F. Lantelme, R. Lindstrom, R. Badour-Hadjean, S. Zanna and D. Lincot, Amorphous vanadium oxide films synthesised by ALCVD for lithium rechargeable batteries, *J. Power Sources*, 2006, **160**(1), 592–601.
22 K. Jost, C. R. Perez, J. K. McDonough, V. Presser, M. Heon, G. Dion and Y. Gogotsi, Carbon coated textiles for flexible energy storage, *Energy Environ. Sci.*, 2011, **4**(12), 5060–5067.
23 J. Bae, M. K. Song, Y. J. Park, J. M. Kim, M. Liu and Z. L. Wang, Fiber supercapacitors made of nanowire–fiber hybrid structures for

wearable/flexible energy storage, *Angew. Chem., Int. Ed.*, 2011, **50**(7), 1683–1687.
24 L. Hu, W. Chen, X. Xie, N. Liu, Y. Yang, H. Wu, Y. Yao, M. Pasta, H. N. Alshareef and Y. Cui, Symmetrical MnO(2)-carbon nanotube-textile nanostructures for wearable pseudocapacitors with high mass loading, *ACS Nano*, 2011, **5**(11), 8904–8913.
25 M. Zhang, S. L. Fang, A. A. Zakhidov, S. B. Lee, A. E. Aliev, C. D. Williams, K. R. Atkinson and R. H. Baughman, Strong, transparent, multifunctional, carbon nanotube sheets, *Science*, 2005, **309**(5738), 1215–1219.
26 J. N. Barisci, G. G. Wallace and R. H. Baughman, Electrochemical studies of single-wall carbon nanotubes in aqueous solutions, *J. Electroanal. Chem.*, 2000, **488**(2), 92–98.
27 G. Lota, K. Fic and E. Frackowiak, Carbon nanotubes and their composites in electrochemical applications, *Energy Environ. Sci.*, 2011, **4**(5), 1592–1605.
28 G. Zheng, L. Hu, H. Wu, X. Xie and Y. Cui, Paper supercapacitors by a solvent-free drawing method, *Energy Environ. Sci.*, 2011, **4**(9), 3368–3373.
29 Z. Niu, W. Zhou, J. Chen, G. Feng, H. Li, W. Ma, J. Li, H. Dong, Y. Ren, D. Zhao and S. Xie, Compact-designed supercapacitors using free-standing single-walled carbon nanotube films, *Energy Environ. Sci.*, 2011, **4**(4), 1440–1446.
30 K. Evanoff, J. Khan, A. A. Balandin, A. Magasinski, W. J. Ready, T. F. Fuller and G. Yushin, Towards ultrathick battery electrodes: aligned carbon nanotube-enabled architecture, *Adv. Mater.*, 2011, **24**(4), 533–537.
31 L. Whittaker, J. M. Velazquez and S. Banerjee, A VO-seeded approach for the growth of star-shaped VO(2) and V(2)O(5) nanocrystals: facile synthesis, structural characterization, and elucidation of electronic structure, *CrystEngComm*, 2011, **13**(17), 5328–5336.
32 J. Qi, G. Ning, Y. Zhao, M. Tian, Y. Xu and H. Hai, Synthesis and characterizationof V(2)O(3) microcrystal particles controlled by thermodynamic parameters, *Mater. Sci.-Pol.*, 2010, **28**(2), 535–543.
33 T.-D. Nguyen and T.-O. Do, Solvo-hydrothermal approach for the shape-selective synthesis of vanadium oxide nanocrystals and their characterization, *Langmuir*, 2009, **25**(9), 5322–5332.
34 J. S. Anderson and S. Khan, Phase equilibria in vanadium–oxygen system, *J. Less Common Met.*, 1970, **22**(2), 209.
35 X. J. Wang, H. D. Li, Y. J. Fei, X. Wang, Y. Y. Xiong, Y. X. Nie and K. A. Feng, XRD and Raman study of vanadium oxide thin films deposited on fused silica substrates by RF magnetron sputtering, *Appl. Surf. Sci.*, 2001, **177**(1–2), 8–14.
36 P. Tan, S. Dimovski and Y. Gogotsi, Raman scattering of non-planar graphite: arched edges, polyhedral crystals, whiskers and cones, *Philos. Trans. R. Soc. London, Ser. A*, 2004, **362**, 2289–2310.
37 C. Thomsen and S. Reich, Double resonant Raman scattering in graphite, *Phys. Rev. Lett.*, 2000, **85**(24), 5214–5217.
38 S. H. Lee, H. M. Cheong, M. J. Seong, P. Liu, C. E. Tracy, A. Mascarenhas, J. R. Pitts and S. K. Deb, Raman spectroscopic studies of amorphous vanadium oxide thin films, *Solid State Ionics*, 2003, **165**(1–4), 111–116.
39 C. Portet, G. Yushin and Y. Gogotsi, Electrochemical performance of carbon onions, nanodiamonds, carbon black and multiwalled nanotubes in electrical double layer capacitors, *Carbon*, 2007, **45**(13), 2511–2518.
40 Y. Korenblit, A. Kajdos, W. C. West, M. C. Smart, E. J. Brandon, A. Kvit, J. Jagiello and G. Yushin, *In situ* studies of ion transport in microporous supercapacitor electrodes at ultralow temperatures, *Adv. Funct. Mater.*, 2012, DOI: 10.1002/adfm.201102573.
41 L. Wei, M. Sevilla, A. B. Fuertesc, R. Mokaya and G. Yushin, Hydrothermal carbonisation of abundant renewable natural organic chemicals for high-performance supercapacitor electrodes, *Adv. Energy Mater.*, 2011, **1**, 356–361.
42 L. Wei, M. Sevilla, A. B. Fuertes, R. Mokaya and G. Yushin, Polypyrrole-derived activated carbons for high-performance electrical double-layer capacitors with ionic liquid electrolyte, *Adv. Funct. Mater.*, 2011, **22**(4), 827–834.
43 M. Rose, Y. Korenblit, E. Kockrick, L. Borchardt, M. Oschatz, S. Kaskel and G. Yushin, Hierarchical micro- and mesoporous carbide-derived carbon as high performance electrode material in supercapacitors, *Small*, 2011, 1108–1117.
44 Y. Korenblit, M. Rose, E. Kockrick, L. Borchardt, A. Kvit, S. Kaskel and G. Yushin, High-rate electrochemical capacitors based on ordered mesoporous silicon carbide-derived carbon, *ACS Nano*, 2010, **4**(3), 1337–1344.
45 A. Kajdos, A. Kvit, F. Jones, J. Jagiello and G. Yushin, Tailoring the pore alignment for rapid ion transport in microporous carbons, *J. Am. Chem. Soc.*, 2010, **132**(10), 3252.
46 J. Chmiola, G. Yushin, Y. Gogotsi, C. Portet and P. Simon, Anomalous increase in carbon capacitance at pore size below 1 nm, *Science*, 2006, **313**, 1760–1763.
47 J. Chmiola, G. Yushin, R. Dash and Y. Gogotsi, Effect of pore size and surface area of carbide derived carbons on specific capacitance, *J. Power Sources*, 2006, **158**(1), 765–772.
48 A. E. Fischer, K. A. Pettigrew, D. R. Rolison, R. M. Stroud and J. W. Long, Incorporation of homogeneous, nanoscale MnO_2 within ultraporous carbon structures *via* self-limiting electroless deposition: implications for electrochemical capacitors, *Nano Lett.*, 2007, **7**(2), 281–286.
49 L. Wei and G. Yushin, Electrical double layer capacitors with sucrose derived carbon electrodes in ionic liquid electrolytes, *J. Power Sources*, 2011, **196**(8), 4072–4079.
50 I. Kovalenko, D. Bucknall and G. Yushin, Detonation nanodiamond and onion-like carbon—embedded polyaniline for supercapacitors, *Adv. Funct. Mater.*, 2010, **20**(22), 3979–3986.
51 C. Portet, G. Yushin and Y. Gogotsi, Effect of carbon particle size on electrochemical performance of EDLC, *J. Electrochem. Soc.*, 2008, **155**(7), A531–A536.
52 C. Portet, P. L. Taberna, P. Simon and E. Flahaut, Modification of Al current collector/active material interface for power improvement of electrochemical capacitor electrodes, *J. Electrochem. Soc.*, 2006, **153**(4), A649–A653.
53 C. Portet, P. L. Taberna, P. Simon and C. Laberty-Robert, Modification of Al current collector surface by sol–gel deposit for carbon–carbon supercapacitor applications, *Electrochim. Acta*, 2004, **49**(6), 905–912.
54 P. L. Taberna, P. Simon and J. F. Fauvarque, Electrochemical characteristics and impedance spectroscopy studies of carbon–carbon supercapacitors, *J. Electrochem. Soc.*, 2003, **150**(3), A292–A300.